

# Melt Electrowriting of Isomalt for High-Resolution Templating of Embedded Microchannels

Ali Nadernezhad, Matthias Ryma, Hatice Genç, Iwona Cicha, Tomasz Jüngst,\* and Jürgen Groll\*

Fabrication of microchannels using 3D printing of sugars as fugitive material is explored in different fields, including microfluidics. However, establishing reproducible methods for the controlled production of sugar structures with sub-100  $\mu\text{m}$  dimensions remains a challenge. This study pioneers the processing of sugars by melt electrowriting (MEW) enabling the fabrication of structures with so far unprecedented resolution from Isomalt. Based on a systematic variation of process parameters, fibers with diameters down to 20  $\mu\text{m}$  can be fabricated. The flexibility in the adjustment of fiber diameter by on-demand alteration of MEW parameters enables generating constructs with perfusable channels within polydimethylsiloxane molds. These channels have a diameter that can be adjusted from 30 to 200  $\mu\text{m}$  in a single design. Taken together, the experiments show that MEW strongly benefits from the thermal and physical stability of Isomalt, providing a robust platform for the fabrication of small-diameter embedded microchannel systems.

## 1. Introduction


The impressive development of additive manufacturing (AM) is not only based on the freedom in design and the field's progress from prototyping toward manufacturing technologies,

but also on increased accessibility of low budget printers.<sup>[1]</sup> Based on availability, 3D printing activities have increased in a broad range of research areas. Particularly, this led to the acceleration of the development of novel materials for AM, and sugar-based glasses demonstrated their potential in extrusion-based 3D printing, mainly as support material or fugitive inks.<sup>[2–4]</sup>

Especially in tissue engineering, rapid water solubility and ease of removal after printing rendered sugars into valuable fugitive materials for 3D printing as they help to tackle one of the main challenges in the field: perfusion and nutrient support of cell-laden tissue-engineered constructs quickly after fabrication. Miller et al. demonstrated this potential by fabricating delicate microchannels from a mixture of glucose, sucrose, and dextran solutions as a glass ink within cell-laden bulk hydrogels using an extrusion-based approach.<sup>[2]</sup> The dimension of fabricated microchannels ranged from 150 to 750  $\mu\text{m}$ . Since then, several other studies attempted to systematically control and enhance the process of 3D printing of sugars.<sup>[3,5–7]</sup>

Nevertheless, tissue engineering was not the only research field that benefited from AM of fugitive materials. Since the early 2000s, microchannels created with 3D printing of fugitive inks gained increasing attention as an alternative to the traditional soft lithography techniques within the field of microfluidics. These systems address a long-lasting limitation of soft lithography in expanding the microchannel networks from 2D toward 3D. The pioneering work by Theriault et al.<sup>[8]</sup> demonstrated the possibilities of expanding AM toward microfluidics including 3D microchannel networks. Although 3D printing principles promote exciting and new opportunities for microfluidics, soft lithography approaches still hold the advantage over conventional 3D printing technologies such as extrusion printing or stereolithography when it comes to reaching small feature sizes and high surface qualities.<sup>[9,10]</sup> While extrusion-based techniques mostly delivered millifluidic size scales, stereolithography could push the boundaries below 100  $\mu\text{m}$ . However, the commercially available resins and printers to achieve such resolutions are very limited.<sup>[9]</sup> As an alternative to conventional 3D printing technologies, methods such as liquid-filled voids for PolyJet printing<sup>[11]</sup> and Two-Photon direct laser writing polymerization<sup>[12]</sup> allow the fabrication of feature sizes below 50  $\mu\text{m}$ . However, these

A. Nadernezhad, M. Ryma, Dr. T. Jüngst, Prof. J. Groll  
Department of Functional Materials in Medicine and Dentistry  
Institute of Functional Materials and Biofabrication and Bavarian  
Polymer Institute  
University of Würzburg  
Pleicherwall 2, Würzburg 97070, Germany  
E-mail: tomasz.juengst@fmz.uni-wuerzburg.de;  
juergen.groll@fmz.uni-wuerzburg.de  
H. Genç, Prof. I. Cicha  
Department of Otorhinolaryngology  
Head and Neck Surgery  
Section of Experimental Oncology and Nanomedicine (SEON)  
Else Kröner-Fresenius-Stiftung-Professorship  
Universitätsklinikum Erlangen  
Friedrich-Alexander-Universität Erlangen-Nürnberg  
Glueckstr. 10a, Erlangen 91054, Germany

 The ORCID identification number(s) for the author(s) of this article can be found under <https://doi.org/10.1002/admt.202100221>.

© 2021 The Authors. Advanced Materials Technologies published by Wiley-VCH GmbH. This is an open access article under the terms of the Creative Commons Attribution-NonCommercial License, which permits use, distribution and reproduction in any medium, provided the original work is properly cited and is not used for commercial purposes.

DOI: 10.1002/admt.202100221

approaches are limited due to several technology inherent challenges, including the very slow nature of the processes and small build volumes.

These limitations could be overcome by emerging 3D printing technologies, such as melt electrowriting (MEW). MEW provides the opportunity to fabricate delicate microstructures with excellent reproducibility and precision.<sup>[13]</sup> It is an AM process based on the application and manipulation of electrohydrodynamic forces to guide and deposit micrometer-sized fibers ranging between 0.82<sup>[14]</sup> and 180  $\mu\text{m}$ <sup>[15]</sup> in well-defined patterns. A computer-controlled movement of the collector delivers direct control over the deposited pattern. A significant aspect of MEW relevant for the applications involving embedded microchannels relies on the possibility of adjusting process parameters on-the-fly. This makes MEW a one-step fabrication process to realize on-demand feature sizes with great variety. Hrynevich et al. showed that by changing a single MEW factor in a controlled way, the fiber diameter in a simple mesh structure could be altered by one order of magnitude.<sup>[16]</sup> Despite these benefits, MEW is a demanding process concerning the choice of compatible materials. In addition to the high sensitivity of the direct writing process on material changes, the high resolution realized by the small fiber diameters implies extended fabrication times. In particular, the need for materials with low thermal degradation has limited the availability of materials and rendered poly( $\epsilon$ -caprolactone) the gold-standard material for MEW.<sup>[17]</sup> Despite that limitations, MEW has already proved its feasibility to generate micrometer-sized perfusable channels for microfluidic applications based on the fugitive approach.<sup>[18,19]</sup> A limitation yet to be addressed for these approaches is the harsh conditions during the removal of the poly( $\epsilon$ -caprolactone) fibers from the microfluidic devices. Taken together, MEW would benefit from thermally stable, water-soluble materials to advance in the area of microfluidics as those used for conventional extrusion 3D printing.

Although sugar-based inks demonstrated their potential for extrusion 3D printing and might be potential candidates that help overcome the MEW limitations, some technical aspects should be noted. Incorporating water in formulations of sugar glass mixtures can significantly impact the crystallization, viscosity, and degradation kinetics of the sugar glass inks.<sup>[3]</sup> Moreover, the high temperature of the 3D printing process can result in caramelization of the sugars, especially during the extended holding time of the sugar glasses at high temperature during extrusion, which can alter the degree of polymerization.<sup>[20]</sup> This would consequently alter the ink's rheological and mechanical properties during and after the extrusion, resulting in difficulties in reproducibility and control of the fabrication process, especially if a process sensitive to small changes in material's properties such as MEW is considered. A potential sugar candidate to overcome these limitations is Isomalt. Isomalt is a sugar alcohol derived from sucrose in a two-step process and is an approximately equimolar mixture of  $\alpha$ -D-glucopyranosyl-1-6-mannitol (GPM) and  $\alpha$ -D-glucopyranosyl-1-6-sorbitol (GPS). Crystalline Isomalt melts around 142–150 °C, which yields a glassy state after cooling with a glass transition around 60 °C.<sup>[21]</sup> The melting temperature of Isomalt is significantly lower than that of the two isomers, which is attributed to the formation of a simple eutectic between two sugar alcohols.<sup>[22]</sup> An interesting property of Isomalt is that, unlike the other sugar alcohols, Isomalt does not

degrade upon melting.<sup>[22]</sup> This behavior could play a significant role in considering Isomalt for processing methods that involve heating at elevated temperatures during processing, such as MEW. Moreover, Isomalt is a readily available material at low cost, with minimal variations in properties due to regulatory requirements for a sugar substitute in the food industry.

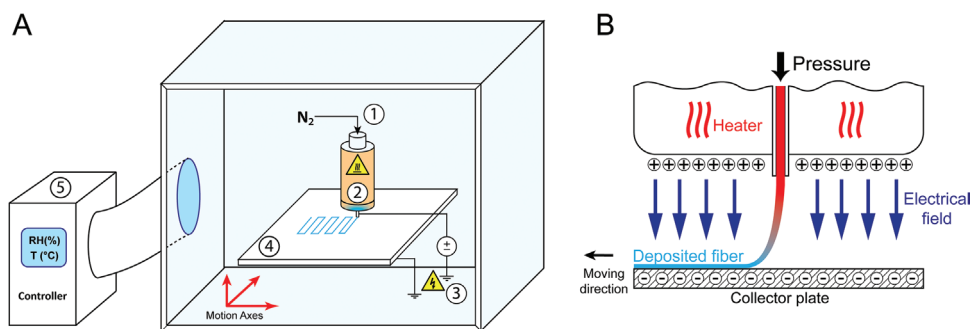
Based on these considerations, we hypothesize that Isomalt is a potential candidate material that enables the fabrication of fugitive fibers within a wide range of dimensions in a reproducible way via MEW. To prove this hypothesis, we show that by systematic variation, precise adjustment, and control of the process parameters, water-soluble Isomalt fibers in the range from 20 to 200  $\mu\text{m}$  diameter can be generated with MEW for the first time. In addition to an analysis of process-related thermal properties of Isomalt and presenting an operational window based on fiber diameter versus MEW process parameters, a preliminary proof-of-concept study demonstrates the flexibility of MEW in combination with Isomalt for the production of perfusable channels potentially relevant for microfluidic applications. The channels generated within PDMS after a water-based dissolution step of the fibers had adjustable shapes and varying diameters.

## 2. Results and Discussion

MEW involves stretching and drawing a very thin fiber driven by the balance between mechanical, gravitational, and electrical forces opposing the viscosity and surface tension of molten material at the nozzle tip.<sup>[23]</sup> Due to the extremely hygroscopic nature of Isomalt, the stability and continuity of the formed jet and, more importantly, the fidelity of deposited Isomalt microfibers would significantly be influenced by environmental conditions. Our preliminary experiments (data not shown) confirmed that at normal laboratory environmental conditions, the extreme hygroscopic nature of Isomalt results in condensation and local dissolution of micrometer-sized Isomalt fibers caused by environmental humidity, and consequently loss of shape and integrity. This effect was more pronounced when the fiber dimensions reached below 100  $\mu\text{m}$ . To enable systematic control over experimental and environmental conditions, all the experiments were conducted in an environmentally monitored chamber (Scheme 1; Figure S1, Supporting Information). By stabilizing the environmental conditions, the reproducibility of the MEW process was ensured, and at the same time, the influence of day-to-day variations of environmental temperature and humidity on the process were minimized.

### 2.1. Characterization of the Isomalt Glass

As thermal properties of any candidate material for MEW play a significant role in the feasibility of the process, thermally stable materials with sufficiently high viscosity are a reasonable choice. Figure 1A,B shows the DSC and TG thermograms of Isomalt. Within the early stage of heating up to 250 °C, only 4.5% of mass loss was observed, which can be attributed to dehydration (Figure 1A). The onset of thermal degradation followed by a massive mass loss was found to be at 250.4 °C. Overall, Isomalt showed excellent thermal



**Scheme 1.** A) Schematics of the MEW device including 1) inlet pressurized nitrogen gas, 2) resistive heating element containing two separate elements for the cartridge and nozzle sections, 3) high-voltage source, 4) collector plate capable of moving in three directions, and 5) environmental chamber controller to set the relative humidity (RH) and temperature of the chamber. B) Drawing to show the configuration of the nozzle and the formed jet due to pulling force of electrical field during fiber deposition.

stability at temperatures below 250 °C, which contrasts with the other sugar candidate materials such as sucrose, fructose, and glucose. Although these sugars are water-soluble and stiff, sucrose-, glucose-, and fructose-based glasses tend to easily oxidize by increasing temperature.<sup>[24]</sup>

The phase transition during heating and cooling of Isomalt was characterized by differential scanning calorimetry (DSC), and the results are shown in Figure 1B. Isomalt is a hygroscopic sugar alcohol that undergoes crystallization upon hydration

during storage. The first heating cycle in DSC showed two peaks, one related to dehydration with the peak at 101.9 °C, and the second peak was due to the melting of the crystal domains. However, the first cooling cycle did not show any crystallization upon cooling, and only a glassy phase until reaching the glass transition was observed. On the other hand, the second heating cycle showed only a glass transition at  $T_g = 54.0$  °C, and further heating did not induce any phase transitions. Sugars can slowly undergo crystallization by being kept above their glass transition

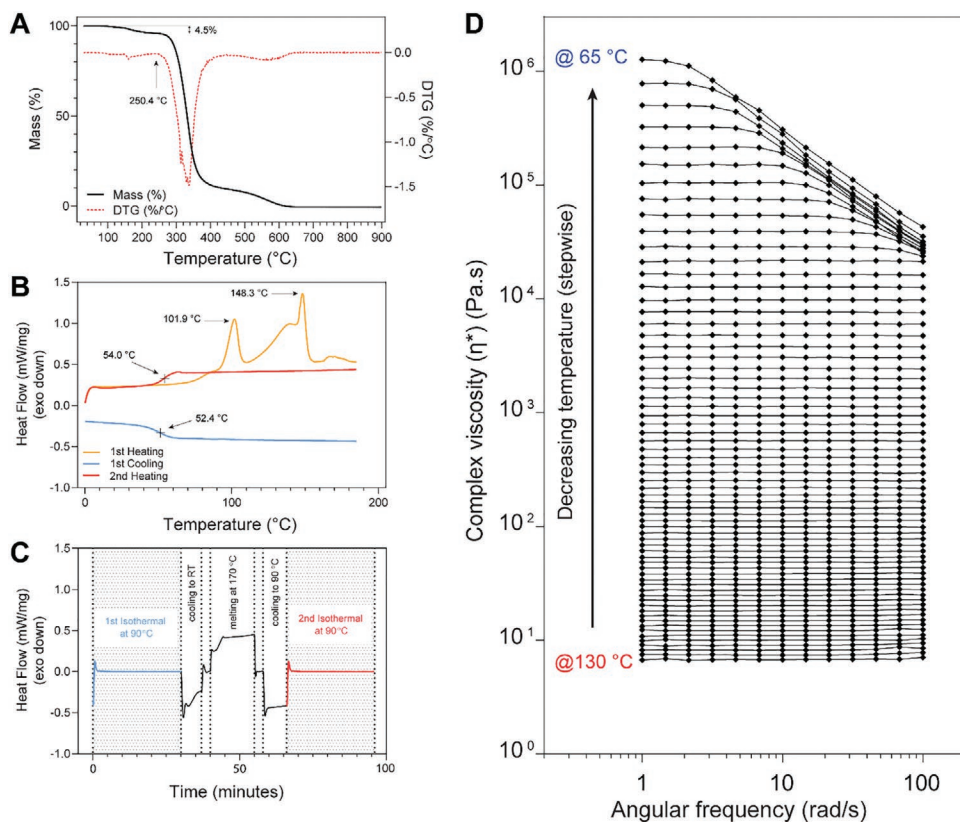


**Figure 1.** Thermal and rheological analysis of Isomalt to investigate compatibility with the MEW process. A) TG profile during heating from 20 to 900 °C. B) DSC profile of first and second heating-cooling cycles showing the glassy state of Isomalt at high temperature. C) DSC profile of Isomalt during cyclic heating-cooling of glass after removing the thermal history. The applied thermal regime mimics the thermal protocol used in MEW. D) Rheological characterization of Isomalt showing a significant increase in complex viscosity over the experimental frequency range by decreasing the temperature of the glass from 130 to 65 °C in a 1 °C per step manner.

for a long time. Moreover, shear is known to accelerate the crystallization of sugars at a glassy state.<sup>[24]</sup> This can cause clogging of the nozzle during the extrusion of glass from a fine nozzle. Unlike the other heat resistive sugars such as lactitol and maltitol, Isomalt is not prone to crystallization even when kept at high temperatures for extended time periods like those expected during fabrication since the crystallization kinetics of Isomalt depends on the hydration degree. Crystallization of Isomalt occurs by the formation of dihydrates, which can be decelerated or almost prevented through dehydration.<sup>[21]</sup> Considering the mechanism and kinetics of crystallization in Isomalt, a single melting step followed by cooling above the glass transition temperature will result in the formation of a stable glassy state, as long as the environmental humidity is monitored and controlled. The thermal stability and consistency in structural properties of Isomalt is a determining factor for the application of this material in processes such as MEW, which rely on continuous deposition of fibers from a material reservoir kept at elevated temperatures. Since the dynamics of processes such as MEW heavily rely on the establishment of a balance between several opposing factors, consistency and stability in the physical properties of the material are of great importance.<sup>[25]</sup> The phenomena such as degradation, polymerization, and crystallization could significantly alter the physical properties of molten or glassy sugars. A cyclic DSC study revealed that after removal of thermal history, Isomalt glass shows a consistent thermal profile during a cyclic heating-cooling regime (Figure 1C). This would further confirm that by following a predefined protocol of removing the thermal history, the physical properties of Isomalt would remain unchanged during MEW processing. In this way, Isomalt offers a stable glassy state at high temperatures in controlled environmental conditions, hence contributing to the stability of the delicate balance governing successful jet formation in MEW.

We hypothesized that by maintaining a glassy state, Isomalt at high temperatures could be extruded or dispensed through a fine nozzle as long as the glass's viscoelastic properties allow the formation of a continuous jet. Rheological characterizations showed that the complex viscosity of Isomalt glass increased about five orders of magnitude by decreasing temperature from 130 to 65 °C (Figure 1D). At high temperatures, Isomalt glass could be easily deformed, and the low viscosity would result in the formation of droplets instead of continuous flow. However, decreasing temperature resulted in a significant increase in viscosity of the glass, followed by exhibiting shear thinning behavior. At 65 °C, the carbohydrate glass showed excessive shear thinning behavior in a wide range of frequencies, with almost one order of magnitude decrease in the value of complex viscosity by sweeping from low to high frequencies.

Considering the thermal and rheological characterization of Isomalt, it was envisioned that, by maintaining the glassy state at a suitable temperature, a continuous flow of material for the jet formation during MEW could be achieved. Initial screening experiments (data not shown) revealed that lowering the set temperature in the two-component heating unit to 90 °C (cartridge zone) and 65 °C (nozzle zone) enabled a continuous flow of glass with proper flexibility of the fiber during the deposition. In this way, the bulk of glass within the syringe cartridge had enough viscosity to tolerate above-atmospheric pressures,

**Table 1.** MEW parameters and the corresponding values.

Parameter	Parameter range/step size	Center value
Applied pressure [bar]	1.0–3.0/0.5	2.0
Applied voltage [kV]	4.0–6.0/0.5	5.0
Tip-to-collector distance [mm]	1.5–3.5/0.5	2.5

while the extruded glass showed pronounced shear-thinning behavior enabling the drawing of very fine microfibers from the nozzle with the aid of the applied electrical field.

## 2.2. Melt Electrowriting of Isomalt

A series of experiments were designed to investigate the processability of Isomalt glass with MEW. Three main parameters of the MEW process were selected and systematically changed between five equidistant levels to obtain and assess an operational window for the production of fibers with different diameters. **Table 1** shows the configuration of constants and the investigated parameters and the corresponding values for each level. The investigated parameter space did not include different temperatures, since our preliminary results (data not shown) indicated that alteration of the temperature of the nozzle results in a significant shift in parameter space, mainly due to significant change in viscoelasticity of Isomalt glass. For this reason, the influence of temperature in resulting MEW fiber diameter was not considered.

Initially, the critical translation speed (CTS) for the production of straight fibers in each experimental set was determined. Determination of CTS, as the transition point between coiled to straight fiber deposition, is crucial in further analysis of printability.<sup>[15]</sup> **Figure 2A** shows the influence of different process parameters on the CTS, accompanied by an exemplary image of the transition between two deposition behaviors at CTS. An increase in CTS value usually indicates the formation of a faster jet during the MEW process. This phenomenon could be explained by considering the correlation between the pulling force induced by the applied electrical field and the mass flow through the nozzle.<sup>[15]</sup> Lower pressure resulted in less mass flow from the nozzle in a constant electrical field intensity, which resulted in whipping and deviation of the formed thin fibers from the designed path.<sup>[15]</sup> Similarly, at a constant pressure, increasing the applied electrical field resulted in more jet instability. To compensate for the induced whipping effect, the collector speed should be increased continuously to enable straight fiber deposition. Decreasing the distance between the nozzle and the collector also resulted in the formation of a faster jet. A faster jet could result from the increased electrical force exerted on the glassy jet, even though the same nominal value of the electrical field was applied to both poles.

After determining CTS for forming a stable jet for each experimental condition, the next step was to investigate the influence of these sets of parameters on the deposited glass fibers' diameter. **Figure 2B** shows the measured values of deposited fibers by varying one process parameter at a time. The collector speed in these experiments was set to be 10% above the CTS value for respective sets, ensuring the observed changes in



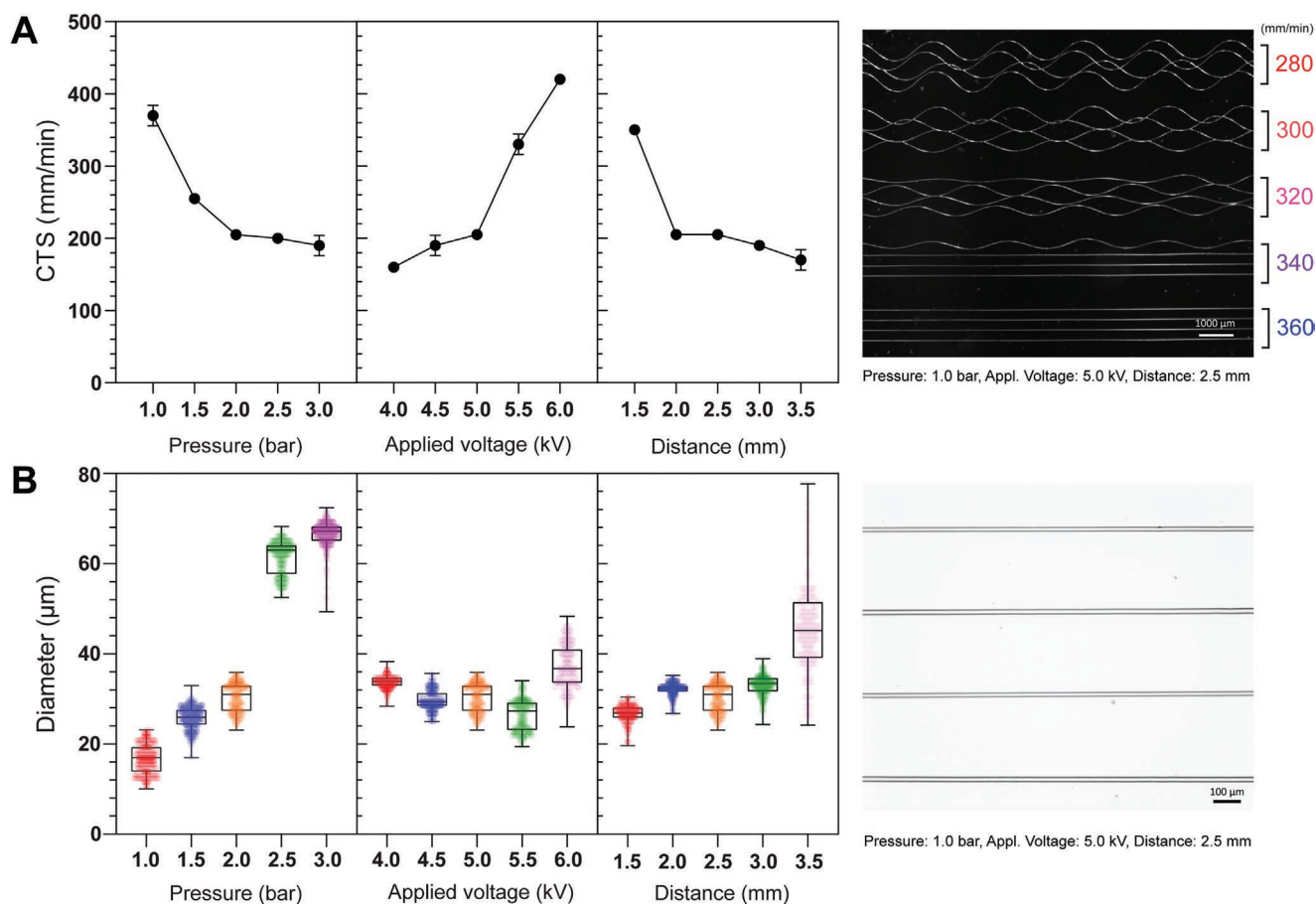


**Figure 2.** Influence of MEW parameters on CTS value and the resulting fiber diameter. A) Variation of CTS based on different parameter combinations in three categories of parameters. An exemplary image of MEW Isomalt glass fibers showing the transition of deposited fibers from coiled to straight by reaching CTS. B) Influence of three MEW parameters on Isomalt glass fiber diameter. The deposition velocity was set to 10% higher than the corresponding CTS value for the respective combination of process parameters. An exemplary image shows the morphology and quality of produced Isomalt fibers deposited in predefined patterns.

fiber diameters are not due to stretching of glassy jet because of mismatch between mass flow and mechanical pulling forces.

In all three categories of parameters, changing the corresponding variable's value resulted in a significant fiber diameter change ( $p < 0.05$ ). Despite the almost uniform change in each experimental category's diameter values, the occurrence of outliers at extreme values of each parametric range resulted in the deviation of measured average values from the expected trends. Increasing the applied pressure to 3.0 bars resulted in an imbalance of mass flow and electrohydrodynamic (EHD) forces applied to the glassy material at the nozzle tip and resulted in a phenomenon termed "pulsing" of the electrified molten jet.<sup>[15]</sup> At these conditions, the diameter of the fiber changes periodically. During the increase of pressure from 2.0 to 2.5 bars, the experimental observations showed that the jet's stability was significantly influenced by increasing the mass flow. However, this impact did not result in an evident periodic change in diameter, as was expected during fiber pulsing. We speculate that the jet's overall stability could be compromised by increasing the pressure above 2.0 bars, but the extent of this effect is proportionally dependent on the applied pressure. Noteworthy, the large variance of the fiber diameter observed

by increasing the applied voltage to 6.0 kV was not mainly due to the pulsing effect. We speculate that the observed behavior could be attributed to the speed of the glassy jet descending upon the collector surface. Given a constant travel distance from the nozzle to the collector, a faster jet would result in a shorter travel time, leading to the deposition of softer glassy fiber with higher temperature. This might cause the local spreading and deformation of the fibers with broader statistical deviations. It should be noted that experimental and computational data showed that in addition to natural convection and radiation, EHD effect could enhance the heat transfer during the landing of the molten jet.<sup>[26]</sup> The possible counter-influence of EHD heat transfer enhancement on the cooling of glassy Isomalt jet could compensate for the shorter cooling period during the landing of high-speed jet, but confirmation of this hypothesis would need detailed characterizations which are not in the scope of this study.

A significant variation in fiber diameter at large tip-to-collector distances was observed. This effect can be attributed to the plasticity of the jet, where the larger distance at constant applied voltage leads to weaker electrohydrodynamic forces and thus a slower landing of the jet. The slower travel speed

promotes lower jet temperature upon landing, causing artifacts in deposited fibers due to mechanical forces induced by the lack of plasticity.

Despite the challenges in stabilizing fibers at the extremes of the investigated experimental window, it was observed that by adjusting easy to control parameters, successful deposition of Isomalt microfibers with reasonable control over the dimension could be achieved. In contrast to conventional extrusion 3D printing, the combined application of electrical and mechanical forces to draw a fine fiber in MEW provides the technical advantage of working with materials with higher inherent viscosity. On one hand, this implies the possibility of lower process temperatures, which is in favor of avoiding the thermally induced deterioration of material's properties. On the other hand, the higher viscosity of the melt or glassy material could potentially enhance the resolution and the stability of the drawn fibers at the same time. The excellent processability of Isomalt by MEW could be correlated with the ease of drawing a thin glassy jet with enough plasticity and viscosity to yield stable fibers with controllable dimensions.

### 2.3. High-Resolution Templating of Microchannels

As mentioned in the introduction, MEW is a powerful method for the fabrication of fibrous constructs with well-ordered microstructure.<sup>[25]</sup> A significant aspect of this technology is the potential to alter the process parameters on-the-fly, meaning that deployment of continuous and on-demand features of the design is possible. Previous studies using poly( $\epsilon$ -caprolactone), the "gold standard" material in MEW, showed that by merely changing the collector's speed, a wide range of fiber diameters between 2 and 50  $\mu\text{m}$  within the same construct could be achieved.<sup>[16]</sup> It has also been shown that a systematic variation of several process parameters enables optimization and parametric prediction of the MEW process.<sup>[27]</sup> With such flexibility in controlling the dimensional features using MEW, fabrication of templating structures from Isomalt could provide the opportunity to create microchannels within a substrate with multiple scales of hierarchy. It should be noted that the experimental window for the fabrication of Isomalt fibers by MEW is not limited to the investigated sets of parameters reported so far in this study and their corresponding ranges. Practically, as long as the balance between mass flow and the electrohydrodynamic forces could be maintained, a stable jet formation would be expected.<sup>[23]</sup>

The Isomalt fibers can be quickly and selectively dissolved by exposure to humidity, or generally an aqueous media. Recent reports on 3D printing of sugars showed that by embedding such structures in a matrix of choice, it was possible to generate channels for different application fields ranging from microfluidics to biofabrication. Selective casting and removal of sacrificial geometries is a well-established method for the generation of hollow structures, including microchannels; however, increasing the design's intricacy would practically limit its applicability.<sup>[9]</sup> In this respect, a fugitive structure made of a water-soluble sugar such as Isomalt with different dimensions and structural complexity levels would significantly extend the manufacturing possibilities. In order to facilitate

the embedment of sacrificial fibers, the MEW of Isomalt was directly performed on PDMS substrates. Although the electrical conductivity of PDMS is less than glass substrate, glass is more prone to undergo polarization in a constant electrical field due to the higher relative permittivity. This combination resulted in almost similar behavior of two substrates, and the jet formation was not significantly impacted. Modeling the electric field distribution and the applied electric potential on each substrate's surface showed consistency in the electric field's distribution and intensity during applying different electrical potentials to the nozzle (Figures S2 and S3, Supporting Information). However, suppose a thorough characterization of the MEW process using a PDMS substrate is desired. In that case, the interested reader is encouraged to follow the similar methodology described in the previous section to derive a more detailed correlation between fiber diameter and MEW parameters.

To investigate the suitability of Isomalt glass fibers produced by MEW for the fabrication of microchannels, intricate designs based on continuous fiber deposition with multiple levels of diameter change were evaluated and transferred to a proof-of-concept study. **Figure 3** shows the region-based alteration of MEW parameters to fabricate a continuous path with diameters varying between 30 and 200  $\mu\text{m}$ . The first region of the microchannel design mimics the conventional inertial focusing/mixing design in conventional microfluidics. The curvature of the channel in this region led to a sequential change in fiber diameter, which might be of interest in specific applications such as continuous inertial focusing of flow or microparticles<sup>[28]</sup> (Video S1, Supporting Information). In the study presented here, that region was added to demonstrate the flexibility of MEW in adjusting and altering the geometry of the deposition pattern. It is worth mentioning that the implementation of this region of the design by MEW was the most demanding portion of the process. The deposition of thick fibers in this region required pushing the MEW process to the limits that were not accessible in the previous section's parameter space. This was mainly due to the restrictions in translation speed and applied voltage imposed by the requirements in Section 2.2. Hence, a change in the parameter space was required. Further on, a region with the gradual reduction in diameter connected to a long microchannel with a fixed value of diameter was produced (Video S2, Supporting Information). A controlled change in the diameter of microchannels provides the possibility to achieve adjustable flow rates within the design, even with a constant inlet pressure or flow rate. This feature might be especially appealing for applications involving the analysis of flow behavior in microfluidics or tissue engineering. The significant technological aspect in the fabrication of such structures lies in the correlations between the actual diameter of the deposited glassy fibers and the on-demand and automated change of MEW parameters implemented within the G-code path plans. By removing the MEW Isomalt fibers from the PDMS matrix using a simple immersion in a water bath, a hollow and perfusable continuous microchannel platform with accurately designed dimensions was produced.

The current literature on templating microchannels using 3D printing of sugar glasses reveals the technological limitations of reaching sub-100  $\mu\text{m}$  dimensions.<sup>[3-7,9,10]</sup> Our demonstrated proof-of-concept study shows that by applying MEW,

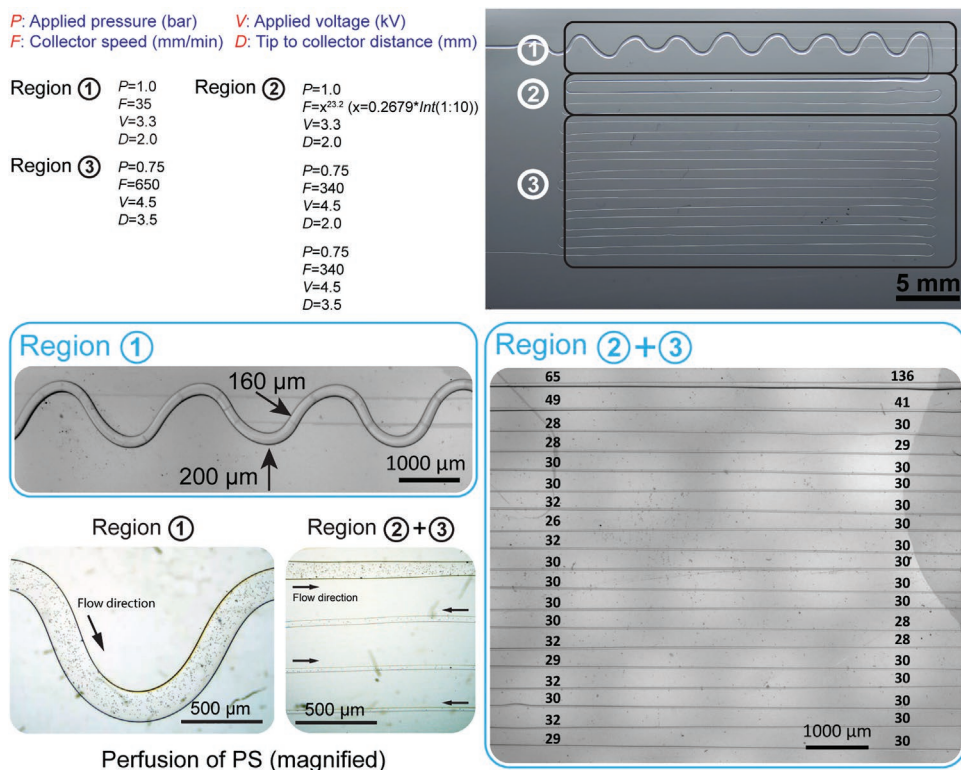


**Figure 3.** An example of an intricate design of microchannels produced from Isomalt glass fibers in a single run, through controlled on-the-fly adjustment of MEW parameters. Regions 1 and 3 of the design mimicked the conventional designs of microchannels in microfluidics with a transition Region 2 connecting both designs in a controlled and stable way. Fiber diameter was decreased from 200  $\mu\text{m}$  in Region 1 to 30  $\mu\text{m}$  in Region 3, with three steps of subtransitions within Region 2 using four easy-to-control parameters. The collector speed in Region 2 was increased exponentially through a ten-step discrete incremental loop. The hollow channels embedded in PDMS could be further perfused with polystyrene (PS) microparticles (magnified subpanels). The perfusion of microchannels and the design induced flow velocities are available in Video S1 and S2 in the Supporting Information.

the resolution can be significantly advanced down to channel diameters of 30  $\mu\text{m}$ . Beyond that, it additionally opens the possibility to fabricate geometries with a wide range of dimensions with size scales ranging from the domain of conventional 3D printing technologies down to the limits of lithography-based techniques in a one-step process.

### 3. Conclusions

We demonstrate the applicability of MEW for the well-controlled production of microfibers from Isomalt. The results show that by precise control over the MEW parameters, Isomalt glass microfibers with a wide range of diameters down to 20  $\mu\text{m}$  can be fabricated. The water solubility of Isomalt provides an easy-to-implement method for the removal of embedded fibers in the final structure, resulting in the formation of perfusable microchannels with on-demand control of the diameter. The flexibility of this process was shown in a proof-of-concept design of microchannels with controlled alteration of fiber diameter between 30 and 200  $\mu\text{m}$  in a one-step fabrication process. This one-step fabrication procedure represents a technological step ahead, which addresses the current limitations in the production of templating structures from fugitive sugar glasses in application areas such as microfluidics.

### 4. Experimental Section

**Materials:** Isomalt (E953) was supplied from a local vendor (TeKa Food GmbH, Germany) and used without further purification. Silicon elastomer kit (Sylgard 184) was purchased from Dow Corning. Aqueous dispersion of 10  $\mu\text{m}$  polystyrene (PS) microbeads was purchased from Sigma-Aldrich.

**Thermal Analysis:** Netzsch DSC204 F1 Phoenix differential scanning calorimetry (DSC) was used to characterize the thermal properties of Isomalt. The heating/cooling rate was set to 10  $\text{K min}^{-1}$ . Thermal gravimetric analysis of Isomalt was performed using Netzsch TG 209 F1 Iris within the temperature range of 20–900  $^{\circ}\text{C}$  with a heating rate of 10  $\text{K min}^{-1}$ .

**Rheology:** Viscoelastic properties of Isomalt at high temperature was characterized through sequential frequency sweeps during 1  $^{\circ}\text{C}$  stepwise cooling from 130 to 65  $^{\circ}\text{C}$ . For this purpose, Anton Paar MCR702 rheometer equipped with 25 mm parallel plate geometry was used. Frequency sweeps between 1 and 100  $\text{rad s}^{-1}$  were performed at each temperature interval while the applied strain was kept constant at 0.1%.

**Imaging:** Optical imaging of the melt electrowritten Isomalt fibers was performed using Discovery V20 stereomicroscope (Carl Zeiss Microscopy GmbH, Germany). Perfusion of microparticles through the embedded channels was photographed with Zeiss Axio Vert. A1 (Carl Zeiss Microscopy GmbH, Germany) inverted microscope equipped with a high-speed camera (Phantom High Speed, Vision Research, USA).

**Melt Electrowriting:** The MEW device (Scheme 1) was enclosed in a closed chamber connected to an environmental controller for temperature and humidity (ACS Discovery, ATT Umweltsimulation GmbH, Germany). The chamber's relative humidity and temperature were set to  $18 \pm 1\%$  and  $39 \pm 1^{\circ}\text{C}$ , respectively. The MEW device included a heated reservoir mounted on a computer-controlled 3-axis platform.

Pressurized nitrogen gas was connected to the melt reservoir through an automated valve. The high-temperature reservoir included two separate sections for heating the syringe-based cartridge and the nozzle with dedicated controllers. The nozzle and the build plate were connected to a computer-controlled high-voltage source (HCP 14-20000, FuG Elektronik GmbH, Germany). A central control unit (Bosch Rexroth AG, Germany) was used to drive the three-axis platform and trigger the corresponding signals for temperature, applied pressure, and applied electrical field controllers as integrated functions during the execution of the G-code path planning. For MEW of carbohydrate glass, glass syringes filled with the granules were placed in the heating unit preheated at 170 °C to ensure removing all the thermal history by complete melting. After 30 min, the heating unit's temperature was gradually decreased to the set process temperature and was kept for 30 min before printing to ensure a thermal equilibrium is reached. The Isomalt fibers were printed on 1.1 mm thick glass slides (VWR, Germany), placed on the stainless-steel collector.

**MEW Process Parameters:** The selected MEW process parameters were systematically changed between five equidistant levels according to Table 1. Only one parameter was changed at a time, and the other variables were set as the center values of corresponding ranges. The critical translation speed (CTS) was first identified for each set of parameters. To ensure deposition of straight fibers and minimize the change in fiber diameter due to stretching of the fibers, the collector velocity for each series of experiments was set to 10% higher than the corresponding CTS value for the respective combination of process parameters. The measured fiber diameters ( $n = 300$ ) from microscopy images were evaluated with a one-way analysis of variance (ANOVA), and the differences with  $p$ -values lower than 0.05 ( $p < 0.05$ ) were considered as statistically significant.

**Numerical Modeling:** The impact of different substrates on the MEW process was modeled numerically in Comsol multiphysics using the AC/DC module (Comsol Inc., USA). The electric field distribution in stationary DC field was done by solving the Maxwell equation with the boundary conditions used based on the experimental parameters. The values of the electrical conductivity and permittivity of glass and PDMS were obtained from the Comsol library and literature.<sup>[29]</sup> The influence of the substrate on electrical field distribution with different applied electrical potentials (4.0–6.0 kV with 500 V increments) was evaluated.

**Fabrication of Templated Microchannels:** Silicon elastomer resin was used to fabricate Polydimethylsiloxane (PDMS) slabs with a thickness of 1 mm. The resin was cast in an aluminum mold and cured at 150 °C for 9 min. The cured slabs were used as substrates during MEW. The Isomalt fibers were directly deposited onto the PDMS surface. During printing, process parameters were extensively altered to precisely control the diameter of deposited fibers based on the design. After printing, the PDMS substrate and the deposited fibers were gently moved to an aluminum mold, and freshly prepared silicon elastomer resin was slowly poured over the printed fibers. The embedded fibers were left at room temperature for 48 h to cure the resin completely. The inlet and outlet points of the resultant structure were generated using a 0.9 mm biopsy punch. The embedded fibers were soaked in Milli-Q water and kept at 60 °C for 24 h for the complete dissolution of Isomalt fibers. The PDMS slab with embedded channels was attached to a plasma-activated microscopy glass slide. The fabricated channels' patency was assessed by perfusion of 0.1 wt% dispersion of 10 μm PS microbeads in 35% PEG 400 solution in Milli-Q water.

## Supporting Information

Supporting Information is available from the Wiley Online Library or from the author.

## Acknowledgements

This work was funded by the Deutsche Forschungsgemeinschaft (DFG, German Research Foundation) with project number 326998133-TRR

225 (subproject B02) and the German Federal Ministry of Education and Research (BMBF) project SOP-Bioprint with contract number 13XP5071A. The authors thank the Industrielle Gemeinschaftsforschung IFG and the Arbeitsgemeinschaft industrieller Forschungsvereinigungen AIF (IGF-Vorhaben No. 19054 N) for the support that enabled to set up the MEW printer used for the study and the European Union for support on printing strategies (European Fund for Regional Development - EFRE Bayern, Bio3D-Druck project 20-3400-2-10). Tomasz Jüngst would also like to thank the European Union for funding by the European Union's Horizon 2020 research and innovation program under grant agreement 874827. All authors thank Christoph Böhm and Juliane C. Kade for their assistance in TG and DSC data acquisition. The assistance and expertise of Andrei Hrynevich and Gernot Hochleitner in designing and setting up the MEW printer are highly appreciated.

Open access funding enabled and organized by Projekt DEAL.

## Conflict of Interest

The authors declare no conflict of interest.

## Data Availability Statement

The data that support the findings of this study are available from the corresponding author upon reasonable request.

## Keywords

embedded templating, melt electrowriting, microfibers, microfluidics, sacrificial printing, sugar glass printing

Received: February 23, 2021

Revised: April 19, 2021

Published online: June 20, 2021

- [1] Y. He, Y. Wu, J. z. Fu, Q. Gao, J. j. Qiu, *Electroanalysis* **2016**, *28*, 1658.
- [2] J. S. Miller, K. R. Stevens, M. T. Yang, B. M. Baker, D.-H. T. Nguyen, D. M. Cohen, E. Toro, A. A. Chen, P. A. Galie, X. Yu, *Nat. Mater.* **2012**, *11*, 768.
- [3] A. Bégin-Drolet, M.-A. Dussault, S. A. Fernandez, J. Larose-Dutil, R. L. Leask, C. A. Hoesli, J. Ruel, *Addit. Manuf.* **2017**, *15*, 29.
- [4] M. Gelber, G. Hurst, T. Comi, R. Bhargava, *Addit. Manuf.* **2018**, *22*, 38.
- [5] G. Gauvin-Rossignol, P. Legros, J. Ruel, M.-A. Fortin, A. Bégin-Drolet, *Heliyon* **2018**, *4*, e00680.
- [6] Y. He, J. Qiu, J. Fu, J. Zhang, Y. Ren, A. Liu, *Microfluid. Nanofluid.* **2015**, *19*, 447.
- [7] A. M. Pollet, E. F. Homburg, R. Cardinaels, J. M. den Toonder, *Micromachines* **2020**, *11*, 43.
- [8] D. Theriault, S. R. White, J. A. Lewis, *Nat. Mater.* **2003**, *2*, 265.
- [9] A. V. Nielsen, M. J. Beauchamp, G. P. Nordin, A. T. Woolley, *Annu. Rev. Anal. Chem.* **2019**, *13*, 45.
- [10] A. K. Au, W. Huynh, L. F. Horowitz, A. Folch, *Angew. Chem., Int. Ed.* **2016**, *55*, 3862.
- [11] A. D. Castiaux, C. W. Pinger, E. A. Hayter, M. E. Bunn, R. S. Martin, D. M. Spence, *Anal. Chem.* **2019**, *91*, 6910.
- [12] T. Bückmann, N. Stenger, M. Kadic, J. Kaschke, A. Frölich, T. Kennerknecht, C. Eberl, M. Thiel, M. Wegener, *Adv. Mater.* **2012**, *24*, 2710.
- [13] P. D. Dalton, *Curr. Opin. Biomed. Eng.* **2017**, *2*, 49.



- [14] G. Hochleitner, T. Jüngst, T. D. Brown, K. Hahn, C. Moseke, F. Jakob, P. D. Dalton, J. Groll, *Biofabrication* **2015**, *7*, 035002.
- [15] G. Hochleitner, J. F. Hümmer, R. Luxenhofer, J. Groll, *Polymer* **2014**, *55*, 5017.
- [16] A. Hrynevich, B. Ş. Elçi, J. N. Haigh, R. McMaster, A. Youssef, C. Blum, T. Blunk, G. Hochleitner, J. Groll, P. D. Dalton, *Small* **2018**, *14*, 1800232.
- [17] J. C. Kade, P. D. Dalton, *Adv. Healthcare Mater.* **2021**, *10*, 2001232.
- [18] J. N. Haigh, Y. m. Chuang, B. Farrugia, R. Hoogenboom, P. D. Dalton, T. R. Dargaville, *Macromol. Rapid Commun.* **2016**, *37*, 93.
- [19] F. Kotz, P. Risch, K. Arnold, S. Sevim, J. Puigmartí-Luis, A. Quick, M. Thiel, A. Hrynevich, P. D. Dalton, D. Helmer, *Nat. Commun.* **2019**, *10*, 1439.
- [20] B. Jiang, Y. Liu, B. Bhandari, W. Zhou, *J. Agric. Food Chem.* **2008**, *56*, 5138.
- [21] B. Borde, A. Cesàro, *J. Therm. Anal. Calorim.* **2001**, *66*, 179.
- [22] H. Cammenga, B. Zielasko, *Thermochim. Acta* **1996**, *271*, 149.
- [23] T. D. Brown, P. D. Dalton, D. W. Huttmacher, *Prog. Polym. Sci.* **2016**, *56*, 116.
- [24] R. W. Hartel, R. Ergun, S. Vogel, *Compr. Rev. Food Sci. Food Saf.* **2011**, *10*, 17.
- [25] T. M. Robinson, D. W. Huttmacher, P. D. Dalton, *Adv. Funct. Mater.* **2019**, *29*, 1904664.
- [26] E. Zhmayev, D. Cho, Y. L. Joo, *Phys. Fluids* **2011**, *23*, 073102.
- [27] C. B. Dayan, F. Afghah, B. S. Okan, M. Yıldız, Y. Menciloglu, M. Culha, B. Koc, *Mater. Des.* **2018**, *148*, 87.
- [28] D. Di Carlo, D. Irimia, R. G. Tompkins, M. Toner, *Proc. Natl. Acad. Sci. USA* **2007**, *104*, 18892.
- [29] H. Shafiee, J. L. Caldwell, M. B. Sano, R. V. Davalos, *Biomed. Micro-devices* **2009**, *11*, 997.